Glutamine synthetase in human carotid plaque macrophages associates with features of plaque vulnerability : An immunohistological study

Sorto, Pia

2022-07

Sorto , P , Mäyränpää , M I , Saksi , J , Nuotio , K , Ijäs , P , Tuimala , J , Vikatmaa , P , Soinne , L , Kovanen , P T & Lindsberg , P J 2022 , ' Glutamine synthetase in human carotid plaque macrophages associates with features of plaque vulnerability : An immunohistological study ' , Atherosclerosis , vol. 352 , pp. 18-26 . https://doi.org/10.1016/j.atherosclerosis.2022.05.0

http://hdl.handle.net/10138/352323
https://doi.org/10.1016/j.atherosclerosis.2022.05.008

Atherosclerosis 352 (2022) 18–26

Contents lists available at ScienceDirect

Atherosclerosis

journal homepage: www.elsevier.com/locate/atherosclerosis

Glutamine synthetase in human carotid plaque macrophages associates with features of plaque vulnerability: An immunohistological study

Pia Sorto [a,*], Mikko I. Mäyränpää [b], Jani Saksi [a], Krista Nuotio [a], Petra Ijäs [a], Jarno Tuimala [c], Pirkka Vikatmaa [d], Lauri Soinne [a], Petri T. Kovanen [e], Perttu J. Lindsberg [a]

[a] Department of Neurology, Neurocenter, Helsinki University Hospital and Clinical Neurosciences, University of Helsinki, Haartmaninkatu 4, 15th floor, P.O. Box 340, 00029, HUS, Helsinki, Finland
[b] Department of Pathology, University of Helsinki and Helsinki University Hospital, Haartmaninkatu 3, P.O. Box 21, 00014, Helsinki, Finland
[c] Unaffiliated
[d] Abdominal Center, Vascular Surgery, Helsinki University Hospital, P.O. Box 440, 00029, HUS, Helsinki, Finland
[e] Wihuri Research Institute, Biomedicum Helsinki, Haartmaninkatu 8, 00290, Helsinki, Finland

ARTICLE INFO

Keywords:
Glutamine synthetase
Glutamate-Ammonia ligase
GLUL
Carotid atherosclerosis
Macrophages
Fibrous cap

ABSTRACT

Background and aims: Glutamine synthetase (GLUL), the sole generator of glutamine, is a metabolic nexus molecule also involved in atherosclerosis. We recently demonstrated a 2.2-fold upregulation of *GLUL* mRNA in stroke-causing carotid plaques when compared with plaques from asymptomatic patients. Here we compared in the same cohort *GLUL* mRNA expression with plaque gross morphology, and the colocalization of immunodetectable GLUL protein with histopathological changes and molecular and mechanical mediators linked to plaque development.

Methods: Endarterectomy specimens from 19 asymptomatic and 24 stroke patients were sectioned longitudinally and immunostained for GLUL, CD68, α-smooth muscle actin, iron, heme oxygenase-1 and CD163, and graded semiquantitatively in every 1 mm^2. The amounts of cholesterol clefts and erythrocytes were graded. The fibrous cap thickness within each 1 mm^2 area was measured. The association between the local pathological findings was analyzed by a hierarchical mixed modelling approach.

Results: The previously found correlation between *GLUL* mRNA and clinical symptomatology was supported by the increased *GLUL* mRNA in diseased tissue and increased local GLUL immunoreactivity in areas with multiple different atherosclerotic changes. A longer symptom-to-operation time correlated with lower *GLUL* mRNA ($R_s = -0.423$, $p=0.050$) but few outliers had a significantly higher *GLUL* mRNA levels, which persisted throughout the post-symptomatic period. Plaque ulceration associated with 1.8-fold higher *GLUL* mRNA ($p=0.006$). Macrophages were the main GLUL immunoreactive cells. GLUL immunostaining colocalized with erythrocytes, iron, CD163, and heme oxygenase-1. The correlations between local variables were consistent in both asymptomatic and stroke-causing plaques. An inverse correlation was found between the fibrous cap thickness and local GLUL immunoreactivity ($p=0.012$). Considerable variability in interplaque expression pattern of GLUL was present.

Conclusions: Our results link connect macrophage GLUL expression with carotid plaque features characterizing plaque vulnerability.

1. Introduction

Several mechanical and biochemical factors have been proposed to lead the progression of an advanced carotid atherosclerotic plaque (CP) into a vulnerable symptom-producing lesion [1]. The event-causing and clinically silent lesions share many histopathological characteristics [2], such as intraplaque hemorrhage (IPH) [3,4] and cholesterol crystals [4, 5]. Local macrophage phenotype might affect the clinically differential behavior of similar CPs. Metabolically and functionally different macrophage subgroups are known to localize in differentially stable plaque areas [6], linking together the nature of local tissue modification processes, the intraplaque localization of macrophages and their metabolic phenotype. The modification of macrophage metabolism might be one of the means to influence plaque stability [7].

* Corresponding author. Department of Clinical Neurosciences, University of Helsinki, Biomedicum Helsinki, Haartmaninkatu 8, FIN-00290, Helsinki, Finland.
E-mail address: pia.sorto@hus.fi (P. Sorto).

https://doi.org/10.1016/j.atherosclerosis.2022.05.008
Received 18 May 2021; Received in revised form 15 April 2022; Accepted 11 May 2022
Available online 18 May 2022

Table 1
The characteristics of the study population and the carotid plaques.

	SCPs[a]	ACPs[b]	p[c]
Patient characteristics	25	19	
Age, y	64.5 ± 7.2	65.4 ± 8.5	0.749
Sex = female, n (%)	6 (24.0%)	10 (52.6%)	0.053
Body Mass Index (kg/m^2)	27.8 ± 4.5	26.9 ± 4.5	0.678
Weight/kg	81.9 ± 16.4	74.5 ± 14.2	0.118
Hypertension = yes, n (%)	18 (72.0%)	11 (57.9%)	0.586
Lower limb atherosclerosis = yes, n (%)	4 (16.0%)	6 (31. %)	0.243
Coronary artery disease, n (%)	8 (32.0%)	9 (47.4%)	0.305
Diabetes, Type 1 or 2, n (%)	8 (32.0%)	5 (26.3%)	0.686
Dyslipidemia (%)	16 (64.0%)	9 (47.4%)	0.177
Smoking = yes, n (%)	5 (20.0%)	4 (21.1%)	0.932
Carotid plaques clinical measurements			
Carotid stenosis % in digital subtraction angiography	79.4 ± 10.1	76.3 (±7.2)	0.126
Days from symptom to operation	51.6 ± 39.2	–	–
Carotid plaque size and gross morphology[e]			
Plaque thickness/μm[d]	2340 ± 1190	2960 ± 1620	0.279
Macroscopic ulceration, n (%)	14 (56.0%)	5 (26.3%)	0.017
Atheromatous core (%)	8 (32.0%)	2 (10.5%)	0.082
Intraplaque hemorrhage (%)	15 (60.0%)	9 (47.4%)	0.327
Plaque calcification (%)	14 (56.0%)	13 (68.4%)	0.453
Intraplaque thrombus (%)	8 (32.0%)	1 (5.3%)	0.026

[a] SCP = symptom-causing carotid plaque.
[b] ACP = asymptomatic carotid plaque.
[c] Mann Whitney *U* test.
[d] Measured from the microscope slide with GLUL immunostaining.
[e] Recorded by the operating vascular surgeon. The significant differences between the groups are underlined.

Glutamine is the most abundant amino acid in the human body [8]. In macrophages, glutamine supports numerous protective and synthetic functions [9–11], and both pro-and anti-inflammatory functional profiles [11]. Glutamine is generated from glutamate and ammonia solely by the enzyme glutamine synthetase (GLUL) [12,13] in a two-step reaction, the rate of which depends on cofactor availability (divalent metal ions), substrate supply, and the expression and activity of the *GLUL* gene [14].

Metabolomic studies have revealed variations in amino acid profiles between patient groups with different cardiovascular outcomes. Importantly, systemic higher glutamine-glutamate-ratio associates with decreased risk of non-fatal stroke, non-fatal myocardial infarction, cardiovascular death, and also with surrogate variables such as elevated blood pressure, triglycerides, blood glucose levels, waist circumference, and risk of diabetes [15–17]. Glutamine transports nitrogen and carbon between body compartments and acts as a nexus molecule in multiple biosynthetic pathways in numerous cell types [8,13,18] (Supplementary Fig. 1). The role of systemic glutamine level alone in the development of arteriopathy and atherosclerosis is controversial [19–22], potentially reflecting the dynamic nature of the plasma glutamine pool, which links metabolic pathways among cells of different organs together, as reflected, for example, by a fast drop of plasma glutamine level in patients with a critical illness [13]. As glutamine supports the macrophage antioxidant glutathione (GSH) production [23] and erythrophagocytosis [24], systemic glutamine availability could affect the CP behavior through modification of macrophage functional phenotype within the lesion.

Our previous microarray study discovered significant upregulation of *GLUL* mRNA in symptom-causing carotid artery plaques (SCPs) when compared with asymptomatic ones (ACPs) [25]. There are no data about GLUL protein expression in carotid atherosclerotic lesions. Here we describe the immunohistochemically detectable GLUL protein expression pattern in the carotid plaques of the same clinically characterized cohort, consisting of advanced symptom-causing and asymptomatic carotid plaques isolated upon surgical endarterectomy [25–27]. We found GLUL to be expressed by macrophages in areas that are exhibit either markers of progression of atherosclerosis or markers of tissue healing/remodelling, all of which were found in both clinically symptomatic and asymptomatic plaques. We propose a role for GLUL and glutamine-linked metabolism of macrophages primarily in CP progression.

2. Patients and methods

Extended methods are described in the Supplementary data.

2.1. Study population and patient selection

Details of patient selection, baseline characteristics (Table 1) and the carotid endarterectomy (CEA) procedure of the Helsinki Carotid Endarterectomy Study conducted during 1995–2000 have been published previously [25–27]. All the CPs used in this study had been removed during the original CEA procedure, and no CPs were obtained later during surgery for, e.g., restenosis. A 15-year follow-up of the same cohort survivors and their risk of future atherothrombotic events has been published previously [28] and the clinical data were included in this analysis. In this study, we selected a subgroup of the cases, 19 being asymptomatic and 25 stroke-causing CPs, all causing a significant (>70%) stenosis in digital subtraction angiography. All patients underwent brain imaging by computed tomography or magnetic resonance imaging. The symptom status of the plaque was defined preoperatively by a stroke neurologist in clinical examination. The operating vascular surgeon sliced the lesion longitudinally into 5 sections and recorded the gross morphology of the CP (ulceration, IPH, intraplaque thrombus, atheroma, calcification). One of the sections was used for microarray analysis and one was fixed in Carnoy's fluid and embedded in paraffin. All CPs represented complicated AHA class IV lesions, as defined in subsequent microscopic evaluation. Each study patient had given written informed consent upon recruitment. The study protocol was approved by the Ethics Committees of the Departments of Neurology and Surgery of the Helsinki University Central Hospital and conforms to the ethical guidelines of the 1975 Declaration of Helsinki. For the details of the selection of the CP subgroup and its relationship to the previous DNA microarray analysis subgroup [25], see the Supplementary data.

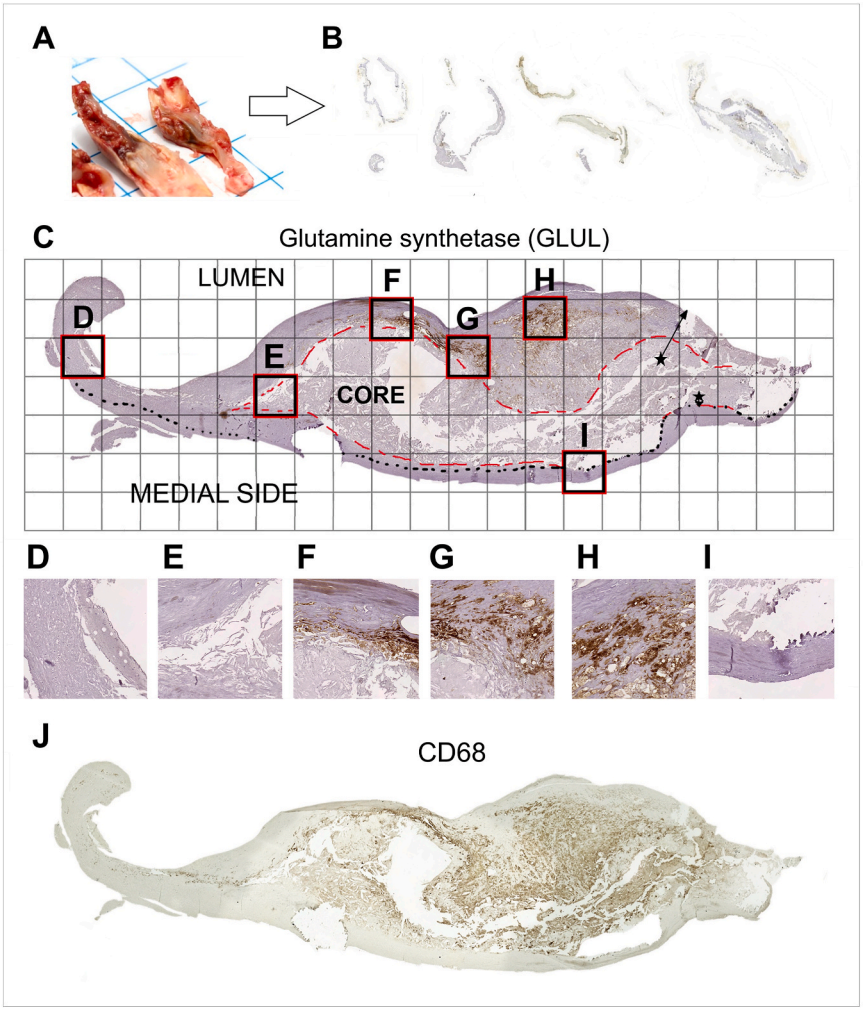

Fig. 1. The microscopical evaluation of the carotid plaques.
Schematic representation illustrating plaque sample preparation after carotid endarterectomy and immunohistochemical analysis method, with carotid plaque sections stained for GLUL and CD68 as examples. (A) The removed CP was dissected longitudinally and evaluated for the gross morphology. One of the sections was fixated with Carnoy's fluid and embedded in paraffin. (B) The samples varied greatly in size and shape. The orientation of the plaque was defined by the medial elastin fibers. The flow direction was not known. (C) A grid was placed on each photomicrograph with computer software and scaled according to the 1 mm scale bar applied to the photomicrograph during image acquisition. The distance of the center of each ROI from either the endothelium or from the intima-media-border was measured from the photo, depending on which one was closer (black stars). Each ROI from the GLUL staining was classified according to its dominant histopathological features (D–I). (D) A 'tunica intima' ROI representing thickened intima outside the plaque lesion, here showing thrombotic mass of unknown age on endothelium. (E) A 'core' ROI, with acellular atheromatous mass and cholesterol clefts. (F) A 'cap' ROI, containing part of the fibrous cap overlying the atheromatous mass, and here a collection of GLUL immunoreactive cells. The fibrous cap thickness was measured at its thickest and thinnest part. The mean value of these measurements was the local cap thickness in the ROI. (G) An 'edge' ROI, containing the perinecrotic zone surrounding the core, here showing a vital intima with more preserved tissue architecture transitioning to the acellular amorphous necrotic mass, also with GLUL immunoreactive cells with macrophage foam cell morphology. (H) An 'inflammation' ROI with a collection of GLUL immunoreactive cells with macrophage appearance, also showing CD68 immunoreactivity (J), but not located in the perinecrotic zone. Only the amount of vital, clearly delineated cells was taken into account, and the amount of nuclei visible in the Prussian blue section was used to support the estimation of the macrophage amount if needed. The overall cellularity was recorded from the Prussian blue section. (I) A 'tunica media' ROI showing mainly medial elastin fibers and remnants of a calcified nodule. The semiquantitative GLUL expression level was recorded from each ROI from 0 to 3 (0 = 0, 1 = +, 2 = ++, 3 = +++). The amount of erythrocyte remnants (0–3), cholesterol clefts (0–3) and calcification (0,1) were recorded from the GLUL section. (J) Adjacent sections with matching morphology stained for CD68 (here), smooth muscle cells, iron, heme oxygenase-1 and CD163 were graded in the same ROIs. Paraffin sections, the brown indicates DAB-labeled anti-GLUL/anti-CD68. Red dashed line = atheromatous core. Black dots: intima-media-border. Black star = the center of the ROI. Black star with an arrow: distance from the center of the ROI either to the endothelium or to the intima-media border.

2.2. Immunohistochemistry

Adjacent 4 μm paraffin sections were immunostained for GLUL, CD68, or α-smooth muscle actin for smooth muscle cells (SMCs). Identically processed normal liver tissue was used as positive control tissue for the CPs. Human dermis served as negative control tissue with only minor immunoreactivity in the basal cell layer. The control tissues were mounted on the same slide with the CP sections. Adjacent slices from the same CPs have been previously immunostained for adipophilin [27], CD163, heme oxygenase 1 (HO-1), and tissue iron [26], and the slides with matching morphology, i.e. adjacent sections from the same CPs, were analyzed in this study. For a detailed description of the immunohistochemical protocols, see the Supplementary data.

2.3. Light microscopy

To investigate the relationship between GLUL protein immunostaining patterns and the other local cellular and biochemical factors within the CP, we applied regional histopathological analysis or the "ROI" (Region Of Interest) method (Fig. 1) [27,29,30]. One researcher (P.S.) performed the immunohistochemical grading blinded to the clinical data. The photographed microscope slices were mapped with a grid of 1000 × 1000 μm squares and each of these areas was graded for the following variables: overall GLUL immunoreactivity (0 = 0, 1 = +, 2 = ++, 3 = +++), cholesterol clefts (0–3), erythrocytes (0–3), calcification (0/1), intra-and extracellular tissue iron (0–3), and the number of nuclei (0–3). The immunoreactivity for CD68 (0–3), α-actin (0–3), HO-1 (0–3) and CD163 (0–3) were recorded from adjacent slices.

All ROIs were classified according to their dominant histopathology into ROIs representing atheromatous core, fibrous cap, perinecrotic zone, inflammatory cell infiltrate, thickened intima, or tunica media (Fig. 1). The thickness of the fibrous cap in each cap-ROI was measured with 50 μm resolution steps so that the resulting thickness was the mean value between the thickest and thinnest measure of the cap within the ROI. For the details of the plaque measurements, see the Supplementary data.

2.4. DNA microarray and quantitative Real-TIME RT-PCR for GLUL mRNA

The protocols for DNA microarray and quantitative Real-TIME RT-PCR for *GLUL* mRNA have been previously published, as well as *GLUL* mRNA association with CP morphological features and clinical risk factors [25]. The mRNA data combined with the novel immunohistochemical data of this study is from the previous study [25]. The relationship of mRNA expression to the aforementioned variables as well as to the follow-up-data of the future atherothrombotic events of the same cohort has been analyzed for the CP subgroup that was the focus of this study [28].

2.5. ELISA

In the non-diluted (1:1) plaque lysates, the GLUL protein mass proportion was maximally 0,000201% of the total plaque protein (n = 29) (Human Glutamine Synthetase ELISA kit LF-EK1085, Abfrontier, Seoul, South Korea). As the quantities were located in the extreme low end of the standard curve of the used ELISA, we excluded them from final analyses.

2.6. Statistical analysis

For correlation analyses, either a nonparametric (Spearman rank correlation) or a parametric (Pearson correlation) correlation coefficient was used where applicable. For comparisons of two groups, a nonparametric Mann-Whitney's *U* test was used (IBM SPSS Statistics 24; IBM, Armonk, NY). The ROI statistical analyses were performed with the assistance of a professional statistician (J.T.). Each CP consists of several ROIs, which makes ROIs non-independent. Each ROI is "nested" inside the CP it comes from. This dependency was taken into account by applying a hierarchical mixed modeling approach. It also allows one to assess the effects of explanatory variables and to adjust for the effects of possible confounding factors, just as any other traditionally used regression modeling approach. Depending on the response variable type, a suitable mixed modeling technique was used. For continuous variables, a linear mixed model was applied. For ordinal variables, a cumulative link mixed model was fitted. Continuous variables were, e.g., distance from the lumen of the blood vessel. Ordinal variables were typically results from histological stainings. These models were fitted using R 3.3 software (R foundation for Statistical Computing, Vienna, Austria) and its add-on packages named *nlme* [31], *lme* [32], and *ordinal* [33].

3. Results

3.1. Glutamine synthetase mRNA expression in the CPs

The foundation of this study is our previous finding showing that *GLUL* gene expression in SCPs is significantly higher than in ACPs (a 2.2 -fold difference, p=0.016) [25]. The data have been analyzed in a search

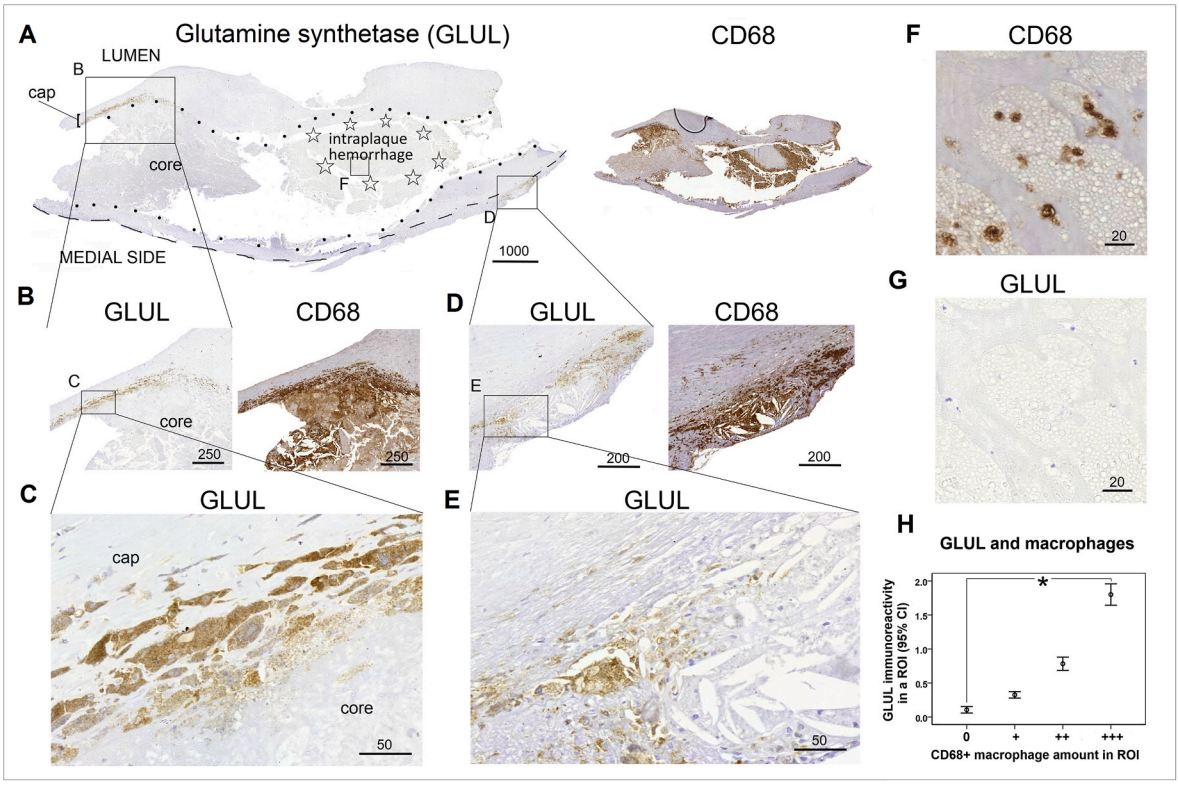

Fig. 2. Glutamine synthetase expression in a subgroup of macrophages within a large lesion.
Glutamine synthetase (GLUL) is expressed by CD68$^+$ macrophages and macrophage foam cells in specific small locations within a large, complex carotid plaque with extravasated erythrocytes. (A) The majority of GLUL immunoreactivity is seen only in two small areas: in the macrophages under the fibrous cap (B and C), and in a small area in the intima-media border (D and E) where atheromatous gruel with cholesterol clefts is surrounded by foamy CD68$^+$ cells of different sizes. (C) In comparison with morphologically distinct and well-defined GLUL+/CD68+ cells located in the fibrous cap, the GLUL+/CD68+ foamy cells with more opaque cell membrane and decreased morphological integrity are located in the transition zone between the cap and the atheromatous core. (F) Within an area rich in extravasated erythrocytes multiple macrophages are seen, but GLUL expression is totally absent from them (G). (H) Statistically significant colocalization of GLUL and macrophages is seen in all ROIs. Paraffin sections, brown indicates DAB-labeled anti-GLUL/anti-CD68. *$p < 0.001$. Dashed line = intima-media border. Black dots = the border of the atheromatous core. Stars = intraplaque hemorrhage with erythrocytes and septas. ROI = 1 mm^2 Region of Interest. Scale bars in micrometers.

for correlations between *GLUL* mRNA expression and the newly investigated gross morphological, microscopical, and molecular features of plaques and the clinical risk factors of patients (Supplementary Table 1).

No associations between *GLUL* mRNA and gender, chronic diseases (Table 1), recent infectious diseases, smoking, laboratory parameters, or medications were found. The *GLUL* mRNA expression level previously measured from the CPs [25] did not correlate with any thrombotic events in the 15-year follow-up data obtained from the same cohort survivors [28]. A longer time delay between the symptom and the operation was associated with lower plaque *GLUL* mRNA expression ($R_s = -0.423$, $p=0.050$) (Supplementary Fig. 3). Higher *GLUL* mRNA was seen in CPs with IPH ($R_s = 0.397$, $p=0.009$) or ulceration (1.8-fold difference, $p=0.006$) when compared to CPs without. CP calcification associated with lower *GLUL* mRNA ($R_s = -0.392$, $p=0.010$).

3.2. Immunodetectable GLUL protein in the CPs

GLUL immunostaining pattern was multiform showing extensive variation between the plaques. GLUL-expression was only intracellular. Certain, often small regions showed clear foci of cell-associated GLUL (Figs. 2D and 3E) while large plaque areas with pathological changes could be almost totally devoid of GLUL (Figs. 2A and 3A). None of the investigated cell types or molecules associated consistently with local GLUL immunoreactivity. GLUL was expressed mainly in caps, perinecrotic zone and inflammatory infiltrate containing ROIs in both SCPs and ACPs (Fig. 4D). The acellular atheromatous core, the thickened intima devoid of inflammatory infiltrates and the tunica media showed almost no GLUL immunoreactive cells (Fig. 4D). Endothelium did not show GLUL immunoreactivity. For a detailed listing of GLUL immunoreactivity associations with other immunohistochemically detected local plaque features, see Supplementary Tables 2–4.

The most dominant GLUL protein immunoreactivity was shown in $CD68^+$ cells displaying morphological features typical of macrophages (Fig. 2). GLUL immunoreactivity in ROIs increased in line with the amount of CD68-expressing cells ($p < 0.001$, Fig. 2H) in all CPs. The appearances of macrophages in the perinecrotic zone showed a gradient of fading GLUL expression in $CD68^+$ cells which appeared to lose their cell membrane and clearly visible structures; these shadowy macrophage remnants seemed to fuse into the atheromatous gruel (Fig. 2B and C). One sample showed GLUL expression in few cells surrounding

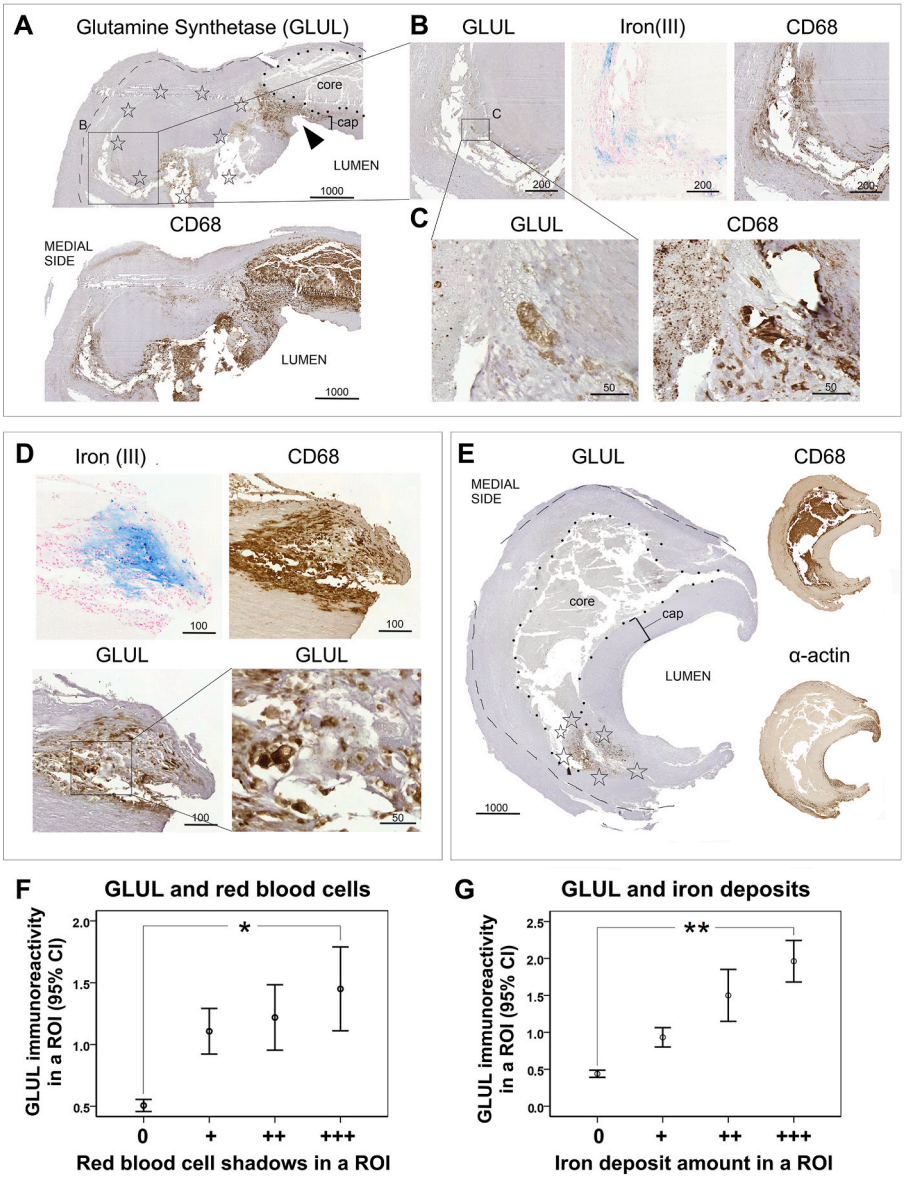

Fig. 3. Glutamine synthetase expression colocalizes with intraplaque hemorrhage components.
Glutamine synthetase (GLUL) immunoreactive macrophages colocalize with erythrocytes and ferric iron deposits, and in an area with cap discontinuity. (A) A large, complicated atheroma shows GLUL immunoreactive macrophages in multiple areas, one of which is an area with a discontinuity of the fibrous cap. (B) Part of the macrophages colocalizing with free and intracellular iron (blue) express GLUL. (C) A GLUL immunoreactive $CD68^+$ cell with ingested erythrocytes, surrounded by $CD68^+$ cells without GLUL expression. (D) Foamy-appearing macrophages colocalizing with extracellular iron are GLUL immunoreactive. (E) A large atheroma is mostly devoid of GLUL immunoreactive cells. GLUL expression does not colocalize at all with smooth muscle α-actin expressing cells. In the GLUL expressing area, remnants of erythrocytes were seen. (F and G) Statistically significant colocalization of GLUL and erythrocytes, and iron. $*p < 0.0001$, $**p < 0.001$. Paraffin sections, the brown indicating DAB-labeled anti-GLUL/anti-CD68 immunoreactivity. Blue in the Prussian blue staining indicates ferric iron deposits. Dashed line = intima-media border. Stars = extravasated erythrocytes and septas. Black dots = border of the atheromatous core. Black arrow = an area where the fibrous cap disappears. ROI = 1 mm^2 Region of Interest. Scale bars in micrometers.

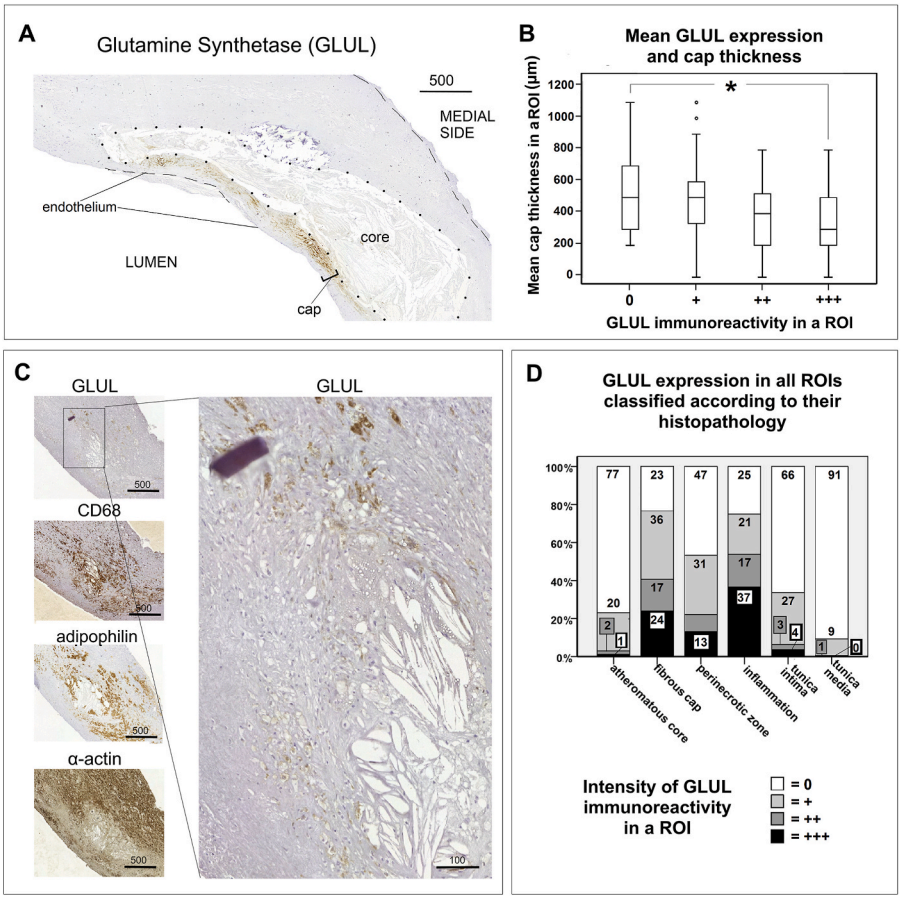

Fig. 4. The localization of glutamine synthetase in the carotid plaques.
Glutamine synthetase (GLUL) expression pattern varied between the samples. (A) In a subgroup of lesions, GLUL was seen only in the fibrous cap siding a cholesterol crystal rich atheroma. (B) In ROIs with thinner fibrous cap, the GLUL expression is higher. (C) GLUL is expressed in a subgroup of cells next to extravasated pool of erythrocytes, where cholesterol clefts are also found. This area contains a large number of macrophages which express adipophilin, a marker for lipid loading, and a large amount of smooth muscle cells. (D) The ROIs with inflammatory cell infiltrates, the ROIs of the perinecrotic zone and fibrous cap areas show highest GLUL immunoreactivity when compared to other plaque areas with different histological features. Histogram showing symptom-causing and asymptomatic plaques combined. See the Supplementary data for the detailed distribution of the GLUL expression in the plaques. *p=0.012. Paraffin sections, the brown indicates DAB-labeled anti-GLUL/anti-CD68. Dashed line = intima-media border. Black dots = border of the atheromatous core. ROI = Region of Interest. Scale bars in micrometers.

erythrocyte membranes blending with a pool of cholesterol clefts (Fig. 4C). Around this area, most of the macrophages, SMCs, and adipophilin-expressing lipid-loaded cells were not expressing GLUL, showing GLUL expression as a property of a small subgroup of macrophages. Throughout the samples, a significant amount of macrophage and foam cell collections did not show GLUL immunoreactivity at all (Fig. 2A, 2F-G, 3E and 4C), revealing heterogeneity in the expression of GLUL even among the macrophages.

In a subgroup of the samples, the only GLUL immunoreactive cells were CD68^{+} cells with macrophage morphology located directly under or within the fibrous cap (Fig. 2A–C and 4A). Higher GLUL immunoreactivity was found in ROIs where the fibrous cap was thinner, and this correlation was linear throughout the material (p=0.012, Fig. 4B). In the cap-ROIs of SCPs, the quantity of cholesterol clefts correlated positively with GLUL immunoreactivity (p=0.004). In SCP ROIs the amount of SMCs decreased when local GLUL expression increased (p=0.001). Typical SMC-appearing cells with α-actin immunoreactivity did not show GLUL expression (Fig. 3E).

GLUL/CD68-expressing cells with erythrophagocyte morphology colocalized morphologically and statistically with extravasated erythrocytes ($p < 0.0001$) and with iron deposits ($p < 0.0001$) (Fig. 3B–D), as well as with CD163 ($p < 0.001$) and HO-1 ($p < 0.001$) (Fig. 3F and G). Macrophage GLUL expression was not observed in all IPHs (Fig. 2A, F-G).

Certain multicellular areas in the perinecrotic zone, that appeared to express both inflammation and tissue remodelling, contained large amounts of nuclei, and high expression of both CD68 and α-actin. In these areas, GLUL expression colocalized also with SMCs; however, differentiation between SMCs and macrophages could not always be done with certainty.

We compared the GLUL protein expression in different depths inside the lesions and assessed its expression in deeper CP domains deemed to contain hypoxia (intraplaque zones deeper than 300 μm from endothelium or from adventitial vasa vasorum) [34]. If a ROI was located mainly within 300 μm depth (superficial), the GLUL expression was lower than in ROIs the surface area of which 50–70% situated beneath 300 μm (moderately deep). However, the ROIs that were completely beneath 300 μm (deepest) showed almost absent GLUL, akin to the absent GLUL expression inside the atheromatous core as well (Supplementary Fig. 4).

4. Discussion

This is the first study describing immunohistochemical detection of glutamine synthetase (GLUL) protein in atherosclerotic lesions. The role of GLUL in the atherosclerotic process remains uncharacterized. Previously we recorded the expression of *GLUL* mRNA to be higher in symptom-causing plaques (SCPs) when compared to non-symptom-causing plaques (ACPs) [25]. Here we both re-analyzed the mRNA expression data and studied the immunohistochemically detected GLUL protein in the above patient cohort. CD68 immunoreactive cells with macrophage morphology were the main GLUL expressive cell type. Both mRNA and protein expression of GLUL associated with pathological CP features typical of plaque vulnerability.

The expression of *GLUL* mRNA was elevated in the diseased tissue, SCPs, ulcerated CPs, and in CPs with IPH, but was lower in lesions with calcification, which is associated with lesion stability. *GLUL* mRNA expression was lower in SCPs with a longer time from symptom to operation/sampling. Previously, a *GLUL* lowering variant was discovered and the risk allele was associated with a 36% increase in the odds of coronary heart disease (CHD) per copy, an effect larger than most of the CHD loci identified in the general population. Importantly, no association was found between this locus and CHD in subjects without diabetes

[35]. To the best of our knowledge, no additional studies of GLUL in relation to cardiovascular diseases exist.

Immunodetectable GLUL protein was expressed mainly by $CD68^+$ macrophages and foam cells. As supported by the mRNA expression data, the areas with the most GLUL immunoreactivity were also morphologically the most advanced regions of the diseased tissue, i.e., areas that are known to contain different proinflammatory/immunostimulatory factors such as cholesterol crystals, erythrocytes and iron, or areas that are deemed to contain hypoxia based on their intraplaque localization. One of the main histological domains of GLUL expressing cells was the perinecrotic zone of the atheroma, where CD68+/GLUL + cells appeared to represent remnants of dying macrophages merging into the existing necrotic core of the atheroma (Fig. 2B and C). Glutamine deficiency has been found to increase monocyte susceptibility to apoptosis [36], and the perinecrotic zone of advanced human atherosclerotic plaques lacks energy metabolites [37]. As an alternative fuel for glucose, glutamine can be directed into energy production through α-ketoglutarate [9,10], to support hypoxic lipogenesis through citrate [38]. As the perinecrotic zone was associated with high GLUL immunoreactivity, this might be linked to the challenges in macrophage energy production or phagocytosis in this area, and potentially to the susceptibility of lipid-engorged macrophages to apoptosis or other types of cellular death [39].

Certain CPs showed GLUL only in their fibrous caps, the cap being the sole area in a large CP with GLUL immunoreactive cells (Fig. 4A). The mean fibrous cap thickness did not differ between SCPs and ACPs. A significant linear correlation was seen between higher GLUL protein expression and the fibrous cap being thinner within a ROI (p=0.012, Fig. 4B). The mean thickness of the cap within the extreme groups with minimum and maximum GLUL in cap ROIs is in line with the Oxford plaque study material, where in non-ruptured caps the mean representative cap thickness was 500 μm and in ruptured plaques 300 μm [40]. Increased GLUL expression was associated with the presence of cholesterol clefts in the fibrous cap ROIs of SCPs (p=0.004), but not in all CP areas that contained cholesterol clefts (perinecrotic zone in Fig. 4A). Cholesterol crystals are known not only to mechanically injure the plaque [5] but also to induce local inflammation by activating the NLRP3 inflammasome in macrophages [41]. GLUL immunoreactivity correlated inversely with the amount of SMCs in all SCP ROIs (p=0.001). Scarcity or total absence of SMCs is a feature associated with CP vulnerability [42]. Taken together, GLUL immunoreactivity was associated with local features indicative of altered cytoarchitecture and endangered tissue strength, particularly in the areas that are central in symptom-generation, i.e. a thin fibrous cap. The proinflammatory (M1-type) macrophages degrade the extracellular matrix [43] and induce apoptosis of the matrix-producing SMCs [44], and thereby promote plaque instability. The M1-macrophage effect is balanced by the activity of the reparatory/inflammation-resolutive macrophages of the M2 phenotype. Previous observations have shown that extracellular glutamine supports M2 polarization [45,46], while a decrease in GLUL activity has been found to lead to polarizing macrophages from the M2-like to the M1-like phenotype [47]. The classification of GLUL-expressing macrophage phenotypes remains a topic for further studies.

The association of *GLUL* mRNA with IPH was confirmed by GLUL immunodetection. GLUL immunoreactive macrophages colocalized with erythrocytes and ferric iron in the CPs (Fig. 3B–D), which are known to fuel local oxidative stress [48]. GLUL-expressing erythrophages were also seen (Fig. 3C). A sample showed a small subgroup of GLUL immunoreactive macrophages surrounding a pool extravasated erythrocytes, potentially converging into cholesterol crystals (Fig. 4C). GLUL colocalized strongly with immunoreactivity of CD163 and HO-1, indicating their co-expression by the same macrophage subgroups. CD163 is one of the M2-type macrophage markers [49,50], expressed by a hemoglobin-scavenging phagocyte. CD163 macrophages induce HO-1 for oxidative heme and iron modification [51]. A previous report indicated that GLUL protein is more susceptible to degradation in pro-oxidative conditions [52]. Inhibition of GLUL enzyme has been found to diminish upregulation of CD163 in macrophages [47]. Moreover, glutamine supplementation can increase the ability of macrophages to express both CD163 and HO-1 [53] and accelerate the process of erythrophagocytosis [24]. A multifaceted role of GLUL in erythrophagocytotic macrophages seems plausible, but needs further studies.

Glutamine protects cells from oxidative stress [54] by supporting cellular glutathione production [23]. A decreased glutathione production has been speculated to lead to the increased CHD risk observed in diabetics with a *GLUL*-lowering variant allele [35]. However, the propensity for systemic GLUL production may not have the same effect as local macrophage GLUL induction in various micromilieus. As discussed above the availability of extracellular glutamine is known to support many of the cellular homeostatic, phagocytosis-related and synthetic processes as it feeds the intracellular glutamate pool and is abundantly available [8,13]. The intracellular GLUL activity on the contrary consumes intracellular glutamate as its substrate (Supplementary Fig. 1), suggesting a more complex role for GLUL in the advanced CP macrophages. To clarify the discrepancy, the distribution of intracellular GLUL activity, a more detailed classification of the GLUL-expressive macrophage phenotypes and the micromilieu conditions such as hypoxia affecting GLUL expression could in the future be studied in differentially challenged cell culture settings and in experimental models with staining series tailored for this kind of analysis, as well as studies into the systemic glutamine dynamics during critical illness and during chronic cardiovascular disease setting, all of them being, however, beyond the scope of the present study.

In conclusion, GLUL is an enzyme expressed by macrophages in atheromatous CP areas with morphological correlates, cell types, and biomolecules that are linked with increased inflammatory activity (IPH, iron), areas that are known to suffer from ATP depletion (perinecrotic zone), oxidative stress (IPH), and compromised tissue integrity and strength (a thinned fibrous cap with a low number of SMCs and increased amount of cholesterol crystals). GLUL is evolutionary highly conserved, being one of the oldest existing enzymes [18,55]. Its product glutamine has the advantage of supporting the survival and multifaceted functions as well as phenotypic variations of macrophages, but the role of intracellular GLUL induction in symptom-causing carotid plaques is unknown. As the *GLUL* mRNA expression declines during the post-symptomatic period, a potential role for GLUL during plaque destabilization, rupture and/or during the post-symptomatic remodelling period can be envisioned. The biochemical and cellular mechanisms by which GLUL and glutamine metabolism could influence these processes in advanced carotid atherosclerotic plaques with dynamic progressive and regressive remodelling is a challenging opportunity for future studies.

Financial support

Jane and Aatos Erkko foundation (P.J.L., #70029), Sigrid Jusélius Foundation (P.J.L., N/a), governmental research funds for Helsinki University Hospital (P.J.L., #TYH2019310), Finnish Medical Foundation (P.S., #1180), Biomedicum Helsinki foundation (P.S., #84).

CRediT authorship contribution statement

Pia Sorto: Conceptualization, Methodology, Investigation, Formal analysis, Writing – original draft. **Mikko I. Mäyränpää:** Conceptualization, Methodology, Writing – original draft. **Jani Saksi:** Conceptualization, Writing – original draft. **Krista Nuotio:** Investigation, Writing – original draft, Writing – review & editing. **Petra Ijäs:** Conceptualization, Writing – original draft. **Jarno Tuimala:** Formal analysis. **Pirkka Vikatmaa:** Writing – review & editing. **Lauri Soinne:** Writing – review & editing. **Petri T. Kovanen:** Writing – original draft, Writing – original draft, Writing – review & editing, Supervision. **Perttu J. Lindsberg:**

Conceptualization, Formal analysis, Writing – original draft, Writing – review & editing, Supervision.

Declaration of competing interest

The authors (P.S., M.I.M., J.S., K.N., P.I., J.T., P.V., L.S., P.T.K., P.J. L.) declare that they have no competing financial interests or personal relationships that could have appeared to influence the work reported in this paper.

Acknowledgements

We thank Taru Puhakka and Nancy Lim for skillful laboratory assistance, Institute of Molecular Medicine in Finland (FIMM) for the webmicroscope facility, and Ville Rantanen for image analysis assistance.

We thank Dr. Matti Jauhiainen for critical reading and comments of the manuscript.

Appendix A. Supplementary data

Supplementary data to this article can be found online at https://doi.org/10.1016/j.atherosclerosis.2022.05.008.

References

[1] V. Fuster, P.R. Moreno, Z.A. Fayad, R. Corti, J.J. Badimon, Atherothrombosis and high-risk plaque: part I: evolving concepts, J. Am. Coll. Cardiol. 46 (2005) 937–954.
[2] D.P.J. Howard, G.W. Van Lammeren, P.M. Rothwell, J.N. Redgrave, F.L. Moll, J.-.P. M. De Vries, et al., Symptomatic carotid atherosclerotic disease: correlations between plaque composition and ipsilateral stroke risk, Stroke 46 (2015) 182–189.
[3] A. Gupta, H. Baradaran, A.D. Schweitzer, H. Kamel, A. Pandya, D. Delgado, et al., Carotid plaque MRI and stroke risk: a systematic review and meta-analysis, Stroke 44 (2013) 3071–3077.
[4] F. Kolodgie, H. Gold, A. Burke, D. Fowler, H. Kruth, D. Weber, et al., Intraplaque hemorrhage and progression of coronary atheroma, N. Engl. J. Med. 349 (2003) 2316–2325.
[5] G.S. Abela, Role of cholesterol crystals in myocardial infarction and stroke, Clin. Lipidol. 5 (2010) 57–69.
[6] M. de Gaetano, D. Crean, M. Barry, O. Belton, M1- and M2-type macrophage responses are predictive of adverse outcomes in human atherosclerosis, Front. Immunol. 7 (2016) 275.
[7] M. Bäck, A. Yurdagul Jr., I. Tabas, K. Öörni, P.T. Kovanen, Inflammation and its resolution in atherosclerosis: mediators and therapeutic opportunities, Nat. Rev. Cardiol. 16 (2019) 389–406.
[8] R. Curi, C.J. Lagranha, S.Q. Doi, D.F. Sellitti, J. Procopio, T.C. Pithon-Curi, et al., Molecular mechanisms of glutamine action, J. Cell. Physiol. 204 (2005) 392–401.
[9] P. Newsholme, R. Curi, S. Gordon, E.A. Newsholme, Metabolism of glucose, glutamine, long-chain fatty acids and ketone bodies by murine macrophages, Biochem. J. 239 (1986) 121–125.
[10] P. Newsholme, R. Curi, T.C. Pithon Curi, C.J. Murphy, C. Garcia, M. Pires de Melo, Glutamine metabolism by lymphocytes, macrophages, and neutrophils: its importance in health and disease, J. Nutr. Biochem. 10 (1999) 316–324.
[11] A. Viola, F. Munari, R. Sanchez-Rodriguez, T. Scolaro, A. Castegna, The metabolic signature of macrophage responses, Front. Immunol. 10 (2019) 1462.
[12] N.P. Curthoys, M. Watford, Regulation of glutaminase activity and glutamine metabolism, Annu. Rev. Nutr. 15 (1995) 133–159.
[13] B.I. Labow, W.W. Souba, Glutamine, World J. Surg. 24 (2000) 1503–1513.
[14] J. Haberle, B. Gorg, A. Toutain, F. Rutsch, J.F. Benoist, A. Gelot, et al., Inborn error of amino acid synthesis: human glutamine synthetase deficiency, J. Inherit. Metab. Dis. 29 (2006) 352–358.
[15] S. Cheng, E.P. Rhee, M.G. Larson, G.D. Lewis, E.L. McCabe, D. Shen, et al., Metabolite profiling identifies pathways associated with metabolic risk in humans, Circulation 125 (2012) 2222–2231.
[16] Y. Zheng, F.B. Hu, M. Ruiz-Canela, C.B. Clish, C. Dennis, J. Salas-Salvado, et al., Metabolites of glutamate metabolism are associated with incident cardiovascular events in the PREDIMED PREvención con DIeta MEDiterránea (PREDIMED) Trial, J. Am. Heart Assoc. 5 (2016), e003755, https://doi.org/10.1161/JAHA.116.003755.
[17] S. Wang, X. Yu, W. Zhang, F. Ji, M. Wang, R. Yang, et al., Association of serum metabolites with impaired fasting glucose/diabetes and traditional risk factors for metabolic disease in Chinese adults, Clin. Chim. Acta 487 (2018) 60–65.
[18] V.R. Young, A.M. Ajami, Glutamine: the emperor or his clothes?, 2486S-7S, J. Nutr. 131 (2001). discussion 2486S-7S.
[19] P. Wurtz, J.R. Raiko, C.G. Magnussen, P. Soininen, A.J. Kangas, T. Tynkkynen, et al., High-throughput quantification of circulating metabolites improves prediction of subclinical atherosclerosis, Eur. Heart J. 33 (2012) 2307–2316.
[20] C. Grajeda-Iglesias, M. Aviram, Specific amino acids affect cardiovascular diseases and atherogenesis via protection against macrophage foam cell formation: review Article, Rambam Maimonides Med. J. 9 (2018).
[21] S.H. Shah, J.R. Bain, M.J. Muehlbauer, R.D. Stevens, D.R. Crosslin, C. Haynes, et al., Association of a peripheral blood metabolic profile with coronary artery disease and risk of subsequent cardiovascular events, Circ. Cardiovasc. Genet. 3 (2010) 207–214.
[22] J. Chen, S. Zhang, J. Wu, S. Wu, G. Xu, D. Wei, Essential role of nonessential amino acid glutamine in atherosclerotic cardiovascular disease, DNA Cell Biol. 39 (2020) 8–15.
[23] M.I. Amores-Sanchez, M.A. Medina, Glutamine, as a precursor of glutathione, and oxidative stress, Mol. Genet. Metabol. 67 (1999) 100–105.
[24] C. Wallace, D. Keast, Glutamine and macrophage function, Metabolism 41 (1992) 1016–1020.
[25] J. Saksi, P. Ijäs, K. Nuotio, R. Sonninen, L. Soinne, O. Salonen, et al., Gene expression differences between stroke-associated and asymptomatic carotid plaques, J. Mol. Med. (Berl.) 89 (2011) 1015–1026.
[26] P. Ijäs, K. Nuotio, J. Saksi, L. Soinne, E. Saimanen, M.-L. Karjalainen-Lindsberg, et al., Microarray analysis reveals overexpression of CD163 and HO-1 in symptomatic carotid plaques, Arterioscler. Thromb. Vasc. Biol. 27 (2007) 154–160.
[27] K. Nuotio, P.M. Isoviita, J. Saksi, P. Ijäs, J. Pitkäniemi, R. Sonninen, et al., Adipophilin expression is increased in symptomatic carotid atherosclerosis: correlation with red blood cells and cholesterol crystals * Online Data, Stroke 38 (2007) 1791–1798.
[28] K. Nuotio, L. Soinne, H. Hänninen, J. Saksi, J. Tuimala, A. Jula, et al., Life-threatening coronary disease is prevalent in patients with stenosing carotid artery disease, Int. J. Stroke 10 (2015) 1217–1223.
[29] M.M. Kockx, K.M. Cromheeke, M.W.M. Knaapen, J.M. Bosmans, G.R.Y. De Meyer, A.G. Herman, et al., Phagocytosis and macrophage activation associated with hemorrhagic microvessels in human atherosclerosis, Arterioscler. Thromb. Vasc. Biol. 23 (2003) 440–446.
[30] P.M. Isoviita, K. Nuotio, J. Saksi, R. Turunen, P. Ijäs, J. Pitkäniemi, et al., An imbalance between CD36 and ABCA1 protein expression favors lipid accumulation in stroke-prone ulcerated carotid plaques, Stroke 41 (2010) 389–393.
[31] J. Pinheiro, D. Bates, S. DebRoy, D. Sarkar, R core team, *nlme: Linear and nonlinear mixed effects models*. R package version 3.1-140. https://CRAN.R-project.org/package=nlme, 2019.
[32] D. Bates, M. Maechler, B. Bolker, S. Walker, Fitting linear mixed-effects models using lme4, J. Stat. Software 67 (2015) 1–48.
[33] R.H.B. Christensen, Ordinal - regression models for ordinal data. R package version 2019. http://www.cran.r-project.org/package=ordinal/, 2019, 4-25.
[34] T. Björnheden, M. Levin, M. Evaldsson, O. Wiklund, Evidence of hypoxic areas within the arterial wall in vivo, Arterioscler. Thromb. Vasc. Biol. 19 (1999) 870–876.
[35] L. Qi, Q. Qi, S. Prudente, C. Mendonca, F. Andreozzi, N. di Pietro, et al., Association between a genetic variant related to glutamic acid metabolism and coronary heart disease in individuals with type 2 diabetes, JAMA 310 (2013) 821–828.
[36] R. Exner, G. Weingartmann, M.M. Eliasen, C. Gerner, A. Spittler, E. Roth, et al., Glutamine deficiency renders human monocytic cells more susceptible to specific apoptosis triggers, Surgery 131 (2002) 75–80.
[37] M. Ekstrand, E. Widell, A. Hammar, L.M. Akyurek, M. Johansson, B. Fagerberg, et al., Depletion of ATP and glucose in advanced human atherosclerotic plaques, PLoS One 12 (2017), e0178877.
[38] R.C. Sun, N.C. Denko, Hypoxic regulation of glutamine metabolism through HIF1 and SIAH2 supports lipid synthesis that is necessary for tumor growth, Cell Metabol. 19 (2014) 285–292.
[39] A. Tajbakhsh, M. Rezaee, P.T. Kovanen, A. Sahebkar, Efferocytosis in atherosclerotic lesions: malfunctioning regulatory pathways and control mechanisms, Pharmacol. Ther. 188 (2018) 12–25.
[40] J.N. Redgrave, J.K. Lovett, P.J. Gallagher, P.M. Rothwell, Histological assessment of 526 symptomatic carotid plaques in relation to the nature and timing of ischemic symptoms: the Oxford plaque study, Circulation 113 (2006) 2320–2328.
[41] K. Rajamäki, J. Lappalainen, K. Öörni, E. Välimäki, S. Matikainen, P.T. Kovanen, et al., Cholesterol crystals activate the NLRP3 inflammasome in human macrophages: a novel link between cholesterol metabolism and inflammation, PLoS One 5 (2010), e11765.
[42] F.D. Kolodgie, K. Yahagi, H. Mori, M.E. Romero, R. Trout Hh, A.V. Finn, et al., High-risk carotid plaque: lessons learned from histopathology, Semin. Vasc. Surg. 30 (2017) 31–43.
[43] A.C. Newby, Metalloproteinase expression in monocytes and macrophages and its relationship to atherosclerotic plaque instability, Arterioscler. Thromb. Vasc. Biol. 28 (2008) 2108–2114.
[44] J.J. Boyle, P.L. Weissberg, M.R. Bennett, Tumor necrosis factor-alpha promotes macrophage-indced vascular smooth muscle cell apoptosis by direct and autocrine mechanisms, Arterioscler. Thromb. Vasc. Biol. 23 (2003) 1553–1558.
[45] A.K. Jha, S.C. Huang, A. Sergushichev, V. Lampropoulou, Y. Ivanova, E. Loginicheva, et al., Network integration of parallel metabolic and transcriptional data reveals metabolic modules that regulate macrophage polarization, Immunity 42 (2015) 419–430.
[46] W. Ren, Y. Xia, S. Chen, G. Wu, F.W. Bazer, B. Zhou, et al., Glutamine metabolism in macrophages: a novel target for obesity/type 2 diabetes, Adv. Nutr. 10 (2019) 321–330.
[47] E.M. Palmieri, A. Menga, R. Martin-Perez, A. Quinto, C. Riera-Domingo, G. De Tullio, et al., Pharmacologic or genetic targeting of glutamine synthetase skews macrophages toward an M1-like phenotype and inhibits tumor metastasis, Cell Rep. 20 (2017) 1654–1666.

[48] E. Nagy, J.W. Eaton, V. Jeney, M.P. Soares, Z. Varga, Z. Galajda, et al., Red cells, hemoglobin, heme, iron, and atherogenesis, Arterioscler. Thromb. Vasc. Biol. 30 (2010) 1347–1353.
[49] S. Gordon, Alternative activation of macrophages, Nat. Rev. Immunol. 3 (2003) 23–35.
[50] T. Roszer, Understanding the mysterious M2 macrophage through activation markers and effector mechanisms, Mediat. Inflamm. 2015 (2015), 816460.
[51] J.H. Thomsen, A. Etzerodt, P. Svendsen, S.K. Moestrup, The haptoglobin-CD163-heme oxygenase-1 pathway for hemoglobin scavenging, Oxid. Med. Cell. Longev. 2013 (2013) 523652.
[52] A.J. Rivett, Preferential degradation of the oxidatively modified form of glutamine synthetase by intracellular mammalian proteases, J. Biol. Chem. 260 (1985) 300–305.
[53] A. Fernandez-Bustamante, A. Agazio, P. Wilson, N. Elkins, L. Domaleski, Q. He, et al., Brief glutamine pretreatment increases alveolar macrophage CD163/heme oxygenase-1/p38-MAPK dephosphorylation pathway and decreases capillary damage but not neutrophil recruitment in IL-1/LPS-insufflated rats, PLoS One 10 (2015), e0130764.
[54] A.R. Kallweit, C.H. Baird, D.K. Stutzman, P.E. Wischmeyer, Glutamine prevents apoptosis in intestinal epithelial cells and induces differential protective pathways in heat and oxidant injury models, JPEN - J. Parenter. Enter. Nutr. 36 (2012) 551–555.
[55] Y. Kumada, D.R. Benson, D. Hillemann, T.J. Hosted, D.A. Rochefort, C. J. Thompson, et al., Evolution of the glutamine synthetase gene, one of the oldest existing and functioning genes, Proc. Natl. Acad. Sci. U. S. A 90 (1993) 3009–3013.